Nonlin. Processes Geophys., 17, 633–649, 2010
www.nonlin-processes-geophys.net/17/633/2010/
doi:10.5194/npg-17-633-2010

Nonlinear Processes in Geophysics

Internal solitary waves: propagation, deformation and disintegration

R. Grimshaw[1], **E. Pelinovsky**[2], **T. Talipova**[2], **and O. Kurkina**[3,4]

[1]Department of Mathematical Sciences, Loughborough University, Leicestershire, UK
[2]Institute of Applied Physics, Nizhny Novgorod, Russia
[3]State University, Higher School of Economics, Nizhny Novgorod, Russia
[4]Institute of Cybernetics, Tallinn University of Technology, Tallinn, Estonia

Received: 1 September 2010 – Revised: 5 November 2010 – Accepted: 5 November 2010 – Published: 17 November 2010

Abstract. In coastal seas and straits, the interaction of barotropic tidal currents with the continental shelf, seamounts or sills is often observed to generate large-amplitude, horizontally propagating internal solitary waves. Typically these waves occur in regions of variable bottom topography, with the consequence that they are often modeled by nonlinear evolution equations of the Korteweg-de Vries type with variable coefficients. We shall review how these models are used to describe the propagation, deformation and disintegration of internal solitary waves as they propagate over the continental shelf and slope.

1 Introduction

Solitary waves are nonlinear localized waves of permanent form, first observed by Russell (1844) as a free surface solitary wave in a canal, and then in a series of experiments. Later, analytical studies by Boussinesq (1871) and Rayleigh (1876) for small-amplitude water waves confirmed Russell's observations. Then Korteweg and de Vries (1895) derived their well-known equation, which contains the "sech"^{2} solitary wave as one of its main solutions. But it was not until the second half of the twentieth century that it was realised that the Korteweg-de Vries (KdV) equation, was, on the one hand, a notable integrable equation, and on the other hand a universal model for weakly nonlinear long waves in a wide variety of physical contexts. The KdV equation, together with various extensions, describes a balance between nonlinear wave-steepening and linear wave dispersion.

Correspondence to: R. Grimshaw
(r.h.j.grimshaw@lboro.ac.uk)

Of principal concern in this paper are the large-amplitude internal solitary waves which propagate in the shallow water of coastal oceans. It is now widely accepted that the basic paradigm for internal waves in shallow seas is based on the KdV equation, first derived in this context by Benney (1966) and Benjamin (1966) and subsequently by many others; for recent reviews see, for instance, Grimshaw (2001), Holloway et al. (2001), Ostrovsky and Stepanyants (2005), Helfrich and Melville (2006), Apel et al. (2007), Grimshaw et al. (2007), or the book by Vlasenko et al. (2005). However, in the coastal ocean, the waves are propagating in a region of variable depth and also through regions of horizontally varying hydrology. In this situation, the appropriate model equation is the variable-coefficient KdV equation

$$A_t + cA_x - \frac{cQ_x}{Q}A + \mu A\,A_x + \delta A_{xxx} = 0\,, \tag{1}$$

Here $A(x,t)$ is the amplitude of the wave, and x, t are space and time variables, respectively. The coefficient $c(x)$ is the relevant linear long wave speed, while $Q(x)$ is the linear modification factor, defined so that $Q^{-2}A^2$ is the wave action flux for linear long waves. The coefficients $\mu(x)$ and $\delta(x)$ of the nonlinear and dispersive terms respectively, are determined by the properties of the basic state. All these coefficients are slowly-varying functions of x. The variable-coefficient KdV equation for water waves was developed by Ostrovsky and Pelinovsky (1970) and later systematically derived by Johnson (1973b), while Grimshaw (1981) gave a detailed derivation for internal waves (see also Zhou and Grimshaw, 1989 and Grimshaw, 2001). The first two terms in (1) are the dominant terms, and hence we can make the transformation

$$A = QU\,, \qquad \xi = \int^x \frac{dx}{c}\,, \qquad s = \xi - t\,. \tag{2}$$

Published by Copernicus Publications on behalf of the European Geosciences Union and the American Geophysical Union.

Substitution into (1) yields, to the same leading order of approximation where (1) holds,

$$U_\xi + \alpha U\, U_s + \lambda U_{sss} = 0 \tag{3}$$

$$\alpha = \frac{Q\mu}{c}\,, \qquad \lambda = \frac{\delta}{c^3}\,. \tag{4}$$

The coefficients α, λ are functions of ξ alone. Note that ξ measures travel time along the spatial path of the wave, while s is a temporal variable measuring the wave phase.

However because internal solitary waves are often of large amplitudes, it is sometimes useful to include a cubic nonlinear term in (1) and (3), which then become, respectively (see the review by Grimshaw, 2001),

$$A_t + cA_x - \frac{cQ_x}{Q}A + \mu A\, A_x + \mu_1 A^2 A_x + \delta A_{xxx} = 0\,, \tag{5}$$

$$U_\xi + \alpha U\, U_s + \beta U^2 U_s + \lambda U_{sss} = 0\,, \tag{6}$$

$$\text{where} \quad \beta = \frac{Q^2\mu_1}{c}\,. \tag{7}$$

Equations (3) and (6), sometimes with various modifications such as with an additional dissipative term, or with a term taking account of the Earth's rotation, have been applied to the study of internal solitary wave wave transformation in the coastal zone by many authors (for instance Cai et al., 2002; Djordjevic and Redekopp, 1978; Grimshaw et al., 2004, 2006, 2007; Holloway et al., 1997, 1999; Hsu et al., 2000; Liu et al., 1988, 1998, 2004; Orr and Mignerey, 2003; Shroyer et al., 2009 and Small, 2001a, b, 2003).

In Sect. 2, we shall present a more detailed description of the derivation of these model equations. Then in Sect. 3, we shall describe the slowly-varying solitary wave solutions of the evKdV equation (6) and in particular examine the behaviour at certain critical points where either α or β vanish. Then in Sect. 4 we shall indicate how these theoretical results can be applied for realistic oceanic conditions, such as those found in the South China Sea.

2 Evolution equations

2.1 Constant depth

The KdV equation is obtained by a weakly nonlinear long wave expansion from the fully nonlinear equations (see Grimshaw, 2001 or Grimshaw et al., 2007). We shall consider only a two-dimensional configuration, see Fig. 1, but initially we assume that the fluid has constant depth h. In the basic state the fluid has density $\rho_0(z)$, a horizontal shear flow $u_0(z)$ in the x-direction, and a pressure field $p_0(z)$ such that $p_{0z} = -g\rho_0$. The density stratification is described by the buoyancy frequency $N(z)$, where

$$N^2(z) = -\frac{g\rho_{0z}}{\rho_0}\,. \tag{8}$$

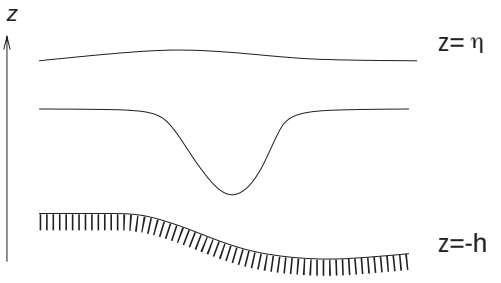

Fig. 1. Coordinate system.

Then, relative to this basic state, the outcome is, to leading order in the small parameter ϵ characterizing the long wave approximation,

$$\zeta \sim \epsilon^2 A(X,T)\phi(z) + \ldots\,, \quad X = \epsilon(x - ct)\,, \quad T = \epsilon^3 t\,. \tag{9}$$

Here ζ is the vertical particle displacement relative to the basic state and the modal function $\phi(z)$ satisfies the system

$$\left\{\rho_0 (c-u_0)^2 \phi_z\right\}_z + \rho_0 N^2 \phi = 0\,, \quad \text{for} \quad -h < z < 0\,, \tag{10}$$

$$\phi = 0 \quad \text{at} \quad z = -h\,, \quad (c-u_0)^2\phi_z = g\phi \quad \text{at} \quad z = 0\,, \tag{11}$$

Equation (10) is the long-wave limit of the Taylor-Goldstein equation, and with the boundary conditions (11), determines the modal function and the linear long wave speed c.

Typically, this boundary-value problem (10, 11) defines an infinite sequence of regular modes, $\phi_n^{\pm}(z)$, $n = 0, 1, 2, \ldots$, with corresponding speeds $c_n^{\pm}$, where "$\pm$" indicates waves with $c_n^+ > u_M = \max u_0$ and $c_n^- < u_M = \min u_0$, respectively. Note that it is useful to let $n = 0$ denote the surface gravity waves for which c scales with $\sqrt{gh}$, and then $n = 1, 2, 3, \ldots$ denotes the internal gravity waves for which c scales with Nh. In general, the boundary-value problem (10, 11) is solved numerically. Typically, the surface mode ϕ_0 has no extrema in the interior of the fluid and takes its maximum value at the surface $z = 0$, while the internal modes $\phi_n^{\pm}(z)$, $n = 1, 2, 3, \ldots$, have n extremal points in the interior of the fluid, and vanish near $z = 0$ (and, of course, also at $z = -h$). Since the modal equations are homogeneous, a normalization condition can be imposed. Here we choose $\phi(z_m) = 1$ where $|\phi(z)|$ achieves a maximum value at $z = z_m$ with respect to z. In this case the amplitude $\epsilon^2 A$ is uniquely defined as the amplitude of ζ (to leading order in ϵ) at z_m.

It can then be shown that, within the context of linear long wave theory, any localised initial disturbance will evolve into a set of outwardly propagating modes, each propagating with the relevant linear long wave speed. Assuming that the speeds $c_n^{\pm}$ of each mode are distinct, it is sufficient for large times to consider just a single mode, as expressed by (9) Then, as time increases, the hitherto neglected nonlinear terms come into play and cause wave steepening. However, this is opposed by the terms representing linear

wave dispersion, also neglected in the linear long wave theory. A balance between these effects emerges as time increases, technically obtained as a compatibility condition at the second order in the expansion. The outcome is the Korteweg-de Vries (KdV) equation for the wave amplitude

$$A_T + \mu A\, A_X + \delta A_{XXX} = 0\,. \tag{12}$$

The coefficients μ and δ are given by

$$I\mu = 3\int_{-h}^{0} \rho_0 (c-u_0)^2 \phi_z^3 dz\,, \tag{13}$$

$$I\delta = \int_{-h}^{0} \rho_0 (c-u_0)^2 \phi^2 dz\,, \tag{14}$$

$$I = 2\int_{-h}^{0} \rho_0 (c-u_0) \phi_z^2 dz\,. \tag{15}$$

Note that after reverting to the original variables x and t, and using (9) Eq. (12) is equivalent to (1) for the case when all coefficients are constant and $Q_x = 0$. The KdV equation (12) is integrable and the long-time evolution from a localized initial condition is a finite number of solitary waves (solitons) and dispersing radiation.

A particularly important special case arises when the nonlinear coefficient μ defined by the expression (13) is close to zero. In this situation, a cubic nonlinear term is needed, and this can be achieved with a rescaling. The optimal choice is to assume that μ is $0(\epsilon)$, and then replace A with A/ϵ in (9); in effect the amplitude parameter is ϵ in place of ϵ^2. The outcome is that the KdV equation (12) is replaced by the extended KdV equation, widely known as the Gardner equation,

$$A_T + \mu A\, A_X + \mu_1 A^2 A_X + \delta A_{XXX} = 0\,,. \tag{16}$$

Again, after reverting to the original variables in (9) Eq. (16) is equivalent to (5) (with $Q_x = 0$). Expressions for the coefficient μ_1 are available, see Grimshaw et al. (2002) and the references therein. Like the KdV equation, (16) is integrable and has solitary wave solutions. There are two independent forms of the eKdV equation (16), depending on the sign of $\delta\mu_1$.

The solitary wave family of the eKdV equation (16) is given by

$$A = \frac{H}{1 + B\cosh K\,(X - VT)}\,, \tag{17}$$

$$\text{where} \quad V = \frac{\mu H}{6} = \delta K^2\,,\; B^2 = 1 + \frac{6\delta\mu_1 K^2}{\mu^2}\,, \tag{18}$$

characterized by a single parameter B. The wave amplitude is $a = H/(1+B)$. For $\delta\mu_1 < 0$, $0 < B < 1$, and the family ranges from small-amplitude waves of KdV-type ("sech^2"-profile) ($B \to 1$) to a limiting flat-topped wave of amplitude $-\mu/\mu_1$ ($B \to 0$), the so-called "table-top" wave, see the upper panel in Fig. 2. For $\delta\mu_1 > 0$ there are two branches; one branch has $1 < B < \infty$ and ranges from small-amplitude KdV-type waves ($B \to 1$), to large waves with a "sech"-profile ($B \to \infty$). The other branch with $-\infty < B < -1$, has the opposite polarity and ranges from large waves with a "sech"-profile when $B \to -\infty$, to a limiting algebraic wave of amplitude $-2\mu/\mu_1$ when $B \to -1$, see the lower panel in Fig. 2 Solitary waves with smaller amplitudes cannot exist, and from the point of view of the associated spectral problem are replaced by breathers, that is, pulsating solitary waves, see, for instance, Pelinovsky and Grimshaw (1997), Grimshaw et al. (1999, 2010), Clarke et al. (2000), Lamb et al. (2007). When $\mu_1 \to 0$, $B \to 1$ and the family reduces to the well-known KdV solitary wave family

$$A = a\,\mathrm{sech}^2\,(K(X - VT))\,, \quad V = \frac{\mu a}{3} = 4\delta K^2\,. \tag{19}$$

Here we have replaced a, K with $2a$, $2K$ to conform with the usual KdV notation.

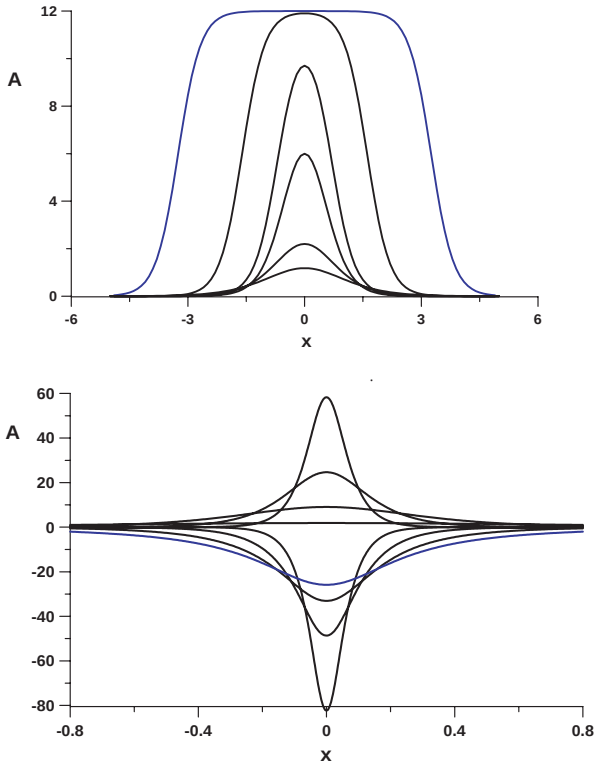

Fig. 2. Solitary wave family (17). The upper panel is for $\mu_1 < 0$ and the lower panel is for $\mu_1 > 0$; in both panels $\mu > 0$, $\delta > 0$.

2.2 Variable background

The derivation sketched above was for the case of constant depth, and when the basic state hydrology is independent of x. But in the ocean, the depth varies and the basic state hydrology may also vary in the propagation direction. These effects can be incorporated into the theory by supposing

that the basic state is a function of the slow variable $\chi = \epsilon^3 x$. That is, $h = h(\chi)$, $u_0 = u_0(\chi, z)$ with a corresponding vertical velocity field $\epsilon^3 w_0(z,\chi)$, a density field $\rho_0(z,\chi)$ a corresponding pressure field $p_0(\chi, z)$ and a free surface displacement $\eta_0(\chi)$. This basic state is assumed to satisfy the full equation set possibly with body forces in the momentum equations. With this scaling, the slow background variability enters the asymptotic analysis at the same order as the weakly nonlinear and weakly dispersive effects. As noted in the Introduction, it is now necessary to replace the variables x, t with ξ, s (2), where it is also convenient to replace the slow variable χ with ξ. An asymptotic analysis analogous to that described above then produces the vKdV equation (1) (Grimshaw, 1981; Zhou and Grimshaw, 1989). The modal system is again defined by (10, 11), but now $c = c(\xi)$ and $\phi = \phi(z,\xi)$, where the ξ-dependence is parametric. The analysis then proceeds as in the constant depth case, but with extra terms corresponding to the slow variability in the basic state, while the compatibility condition then yields the vKdV equation (1) now with variable coefficients $\mu = \mu(\xi), \delta = \delta(\xi)$, but which are again defined by (13, 14, 15) (but the upper limit in the integrals is now $z = \eta_0$ replacing $z = 0$). For the present case of internal waves, we find that the linear modification factor is given by, see Zhou and Grimshaw (1989),

$$Q^2 = \frac{1}{Ic^2}\,, \tag{20}$$

where I is defined by (15). Note also that the expression for Q can also be simply determined by requiring that $Q^{-2}A^2$ should be the wave action flux in the linear long wave limit. The variable-coefficient extended KdV equation (5) is obtained in a similar manner.

We shall conclude this section with some illustrative examples. First consider the case of *surface waves*. We put the density $\rho =$ constant so that then $N^2 = 0$ (8). Then, for the case when there is no background flow so that $u_0 = 0$, $\eta_0 = 0$, we obtain the well-known expressions

$$\phi = \frac{z+h}{h} \quad \text{for} \quad -h < z < 0\,, \quad c = (gh)^{1/2}\,. \tag{21}$$

$$\text{and so} \quad \mu = \frac{3c}{2h}\,, \quad \delta = \frac{ch^2}{6}\,, \quad Q^2 = \frac{1}{2gc}\,. \tag{22}$$

Similarly, for *interfacial waves* in a two-layer fluid, let the density be a constant ρ_1 in an upper layer of height h_1 and $\rho_2 > \rho_1$ in the lower layer of height $h_2 = h - h_1$. That is

$$\rho_0(z) = \rho_1 H(z+h_1) + \rho_2 H(-z-h_1)\,,$$

$$\text{so that} \quad \rho_0 N^2 = g(\rho_2 - \rho_1)\delta(z+h_1)\,.$$

Here $H(z)$ is the Heaviside function and $\delta(z)$ is the Dirac δ-function. Again we assume that there is no background flow ($u_0 = 0$, $\eta_0 = 0$). and we replace the free boundary with a rigid boundary so that the upper boundary condition for $\phi(z)$ becomes just $\phi(0) = 0$. This is a good approximation for oceanic internal solitary waves. Then we find that

$$\phi = \frac{z+h}{h_2} \;\text{ for }\; -h < z < h_1, \;\; \phi = -\frac{z}{h_1} \;\text{ for }\; -h_1 < z < 0,$$
$$c^2 = \frac{g(\rho_2 - \rho_1)h_1 h_2}{\rho_1 h_2 + \rho_1 h_2}\,. \tag{23}$$

Substitution into (13, 14, 15) yields

$$\mu = \frac{3c\left(\rho_2 h_1^2 - \rho_1 h_2^2\right)}{2h_1 h_2(\rho_2 h_1 + \rho_1 h_2)}\,, \quad \delta = \frac{ch_1 h_2(\rho_2 h_2 + \rho_1 h_1)}{6(\rho_2 h_1 + \rho_1 h_2)}\,,$$
$$Q^2 = \frac{1}{2g(\rho_2 - \rho_1)c}. \tag{24}$$

Note that for the usual oceanic situation when $\rho_2 - \rho_1 \ll \rho_2$, the nonlinear coefficient μ for these interfacial waves is negative when $h_1 < h_2$ (that is, the interface is closer to the free surface than the bottom), and is positive in the reverse case. The case when $h_1 \approx h_2$ leads to the necessity to use the extended KdV equation (16), where the coefficient μ_1 is given by

$$\mu_1 = -\frac{3c}{8h_1^2 h_2^2(\rho_1 h_2 + \rho_2 h_1)^2} \left\{\left(\rho_1 h_2^2 - \rho_2 h_1^2\right)^2 + 8\rho_1\rho_2 h_1 h_2 (h_1 + h_2)^2\right\}. \tag{25}$$

Note that $\mu_1 < 0$, and so the eKdV equation (16) for a two-layer fluid always has $\delta\mu_1 < 0$.

However, in a three-layer fluid there are parameter regimes where one or two modes may have $\mu_1 > 0$ (Grimshaw et al., 2002), and there are many cases for real oceanic conditions with smooth stratification and background shear when the parameter $\mu_1 > 0$, see Grimshaw et al. (2004, 2007).

3 Deformation of internal solitary waves

3.1 Slowly varying solitary wave

In general the evKdV equation (6) with variable coefficients $\alpha = \alpha(\xi)$, $\beta = \beta(\xi)\lambda = \lambda(\xi)$ must be solved numerically. However, it is first instructive to consider the slowly-varying solitary wave. This is described in detail in review article by Grimshaw et al. (2007), but for convenience we shall present a brief summary here. The slowly-varying solitary wave is an asymptotic solution based on the assumption that the background state varies slowly relative to a typical wavelength. Formally, we suppose that

$$\alpha = \alpha(\sigma), \;\; \beta = \beta(\sigma), \;\; \lambda = \lambda(\sigma), \;\; \sigma = \kappa\xi, \;\; \kappa \ll 1. \tag{26}$$

We then invoke a multi-scale asymptotic expansion of the form (see Grimshaw, 1979)

$$U = U_0(\psi, \sigma) + \kappa U_1(\psi, \sigma) + \ldots, \tag{27}$$

$$\psi = s - \frac{1}{\kappa}\int^{\sigma} V(\sigma)d\sigma\,. \tag{28}$$

Here ψ is a temporal variable in a frame moving with the speed V. U is defined over the domain $-\infty < \psi < \infty$, and we will require that U remain bounded in the limits $\psi \to \pm\infty$. Since we can assume that $\lambda > 0$ small-amplitude waves will propagate in the negative s-direction, and so we can suppose that $U \to 0$ as $\psi \to \infty$. However, it will transpire that we cannot impose this boundary condition as $\psi \to -\infty$. This procedure is well-known for the vKdV equation (see Johnson, 1973a for the case of water waves, and Grimshaw, 1979 for the general case) and is readily extended to the evKdV equation (see the recent reviews by Grimshaw, 2007 and Grimshaw et al., 2007).

Substitution of (27) into (3) yields,

$$-VU_{0\psi} + \alpha U_0 U_{0\psi} + \beta U_0^2 U_\psi + \lambda U_{0\psi\psi\psi} = 0\,, \tag{29}$$

$$-VU_{1\psi} + \alpha(U_0U_1)_\psi + \beta\left(U_0^2U_1\right)_\psi + \lambda U_{1\psi\psi\psi} = -U_{0\sigma}\,. \tag{30}$$

Equation (29) has the solitary wave solution

$$U_0 = \frac{D}{1 + B\cosh K\psi}\,, \tag{31}$$

$$\text{where}\quad V = \frac{\alpha D}{6} = \lambda K^2\,, \quad B^2 = 1 + \frac{6\lambda\beta K^2}{\alpha^2}\,. \tag{32}$$

When the coefficients are constants, this is just the eKdV solitary wave (17). Here it is a slowly-varying solitary wave as the parameter $B = B(\sigma)$ and hence $a = D/(1+B) = a(\sigma)$, $V = V(\sigma)$, $K = K(\sigma)$. The main aim of the analysis is then to determine how these parameters vary, and this is determined at the next order of the expansion.

We now seek a solution of (30) for $U_1 \to 0$, $\psi \to \infty$ and for which U_1 is bounded as $\psi \to -\infty$. In order to determine the conditions that need to be imposed on the right-hand side of (30) to ensure that such a solution can be obtained, we need to consider the adjoint equation to the homogeneous operator on the left-hand side of (30), which is for the dependent variable $\tilde{U}_1$,

$$-V\tilde{U}_{1\psi} + \alpha U_0\tilde{U}_{1\psi} + \beta U_0^2\tilde{U}_{1\psi} + \lambda\tilde{U}_{1\psi\psi\psi} = 0\,. \tag{33}$$

The required compatibility conditions are then that the right-hand side of (30) should be orthogonal to all linearly independent solutions of the adjoint Eq. (33) which decay at infinity. Two linearly independent solutions of the adjoint Eq. (33) are 1, U_0. While both of these are bounded, only the second solution satisfies the condition that $U_1 \to 0$ as $\psi \to \infty$. The third solution is unbounded as $\psi \to \pm\infty$. Hence only one compatibility condition can be imposed, namely that the right-hand side of (30) is orthogonal to U_0, which leads to

$$P_{0\sigma} = 0 \quad \text{where} \quad P_0 = \int_{-\infty}^{\infty} U_0^2\,d\psi\,. \tag{34}$$

Thus P_0 is a constant, and as the solitary wave (19) has just one free parameter B, this condition suffices to determine its variation.

However, the evKdV equation (6) has two conservation laws

$$\frac{\partial M}{\partial\xi} = 0, \quad M = \int_{-\infty}^{\infty} U\,ds\,, \tag{35}$$

$$\frac{\partial P}{\partial\xi} = 0, \quad P = \int_{-\infty}^{\infty} U^2\,ds\,, \tag{36}$$

for "mass" and "momentum" respectively. In physical terms, (35) is an approximation to the conservation of physical mass, while (36) expresses conservation of wave action flux at the leading order. The condition (34) is easily recognized as the leading order expression for conservation of momentum (36). But since this completely defines the slowly-varying solitary wave, we now see that this cannot simultaneously conserve mass. This is also apparent when one examines the solution of (30) for U_1, from which it is readily shown that although $U_1 \to 0$ as $\psi \to \infty$, $U_1 \to D_1$ as $\psi \to -\infty$ where

$$VD_1 = -M_{0\sigma}\,, \quad \text{where} \quad M_0 = \int_{\infty}^{\infty} U_0\,d\psi\,. \tag{37}$$

This non-uniformity in the slowly-varying solitary wave has been recognized for some time, see, for instance, Knickerbocker and Newell (1978, 1980), Grimshaw (1979) or Grimshaw and Mitsudera (1993) and the references therein. The remedy is the construction of a trailing shelf $U^{(s)}$ of small amplitude $O(\kappa)$ but long length-scale $O(1/\kappa)$, which thus has $O(1)$ mass, but $O(\kappa)$ momentum. It resides behind the solitary wave, and to leading order is given by

$$U^{(s)} = \kappa U^{(s)}(T), \quad \text{for} \quad T = \kappa\xi < \Psi(\sigma) = \int^{\sigma} V(\sigma)d\sigma\,. \tag{38}$$

Here $T = \Psi(\sigma)$ defines the location of the solitary wave. $U^{(s)}(T)$ is independent of σ, and is determined so that the shelf amplitude is just $\kappa D_1(\sigma)$ at the location of the solitary wave, that is $U^{(s)}(\Psi(\sigma)) = D_1(\sigma)$ (37). At higher orders in κ the shelf itself will evolve and may generate secondary solitary waves, see El and Grimshaw (2002) and Grimshaw and Pudjaprasetya (2004). The slowly-varying solitary wave and the trailing shelf together satisfy conservation of mass.

Substitution of the solitary wave (31) into the expression (34) for P_0 yields

$$P_0 = \frac{D^2}{K}\int_{-\infty}^{\infty} \frac{du}{(1 + B\cosh u)^2}\,, \tag{39}$$

$$\text{or} \qquad G(B) = P_0\left|\frac{\beta^3}{\lambda\alpha^2}\right|^{1/2}, \tag{40}$$

$$\text{where} \quad G(B) = \left|B^2 - 1\right|^{3/2}\int_{-\infty}^{\infty} \frac{du}{(1 + B\cosh u)^2}\,. \tag{41}$$

The expression (40) determines the variation of the parameter B since P_0 is a constant, determined by the initial conditions. The integral term in $G(B)$ can be explicitly evaluated,

$$B^2 > 1: \quad G(B) = 2(B^2-1)^{1/2} \mp 4\text{arctan}\sqrt{\frac{B-1}{B+1}}, \qquad (42)$$

$$0 < B < 1: \quad G(B) = 4\text{arctanh}\sqrt{\frac{1-B}{1+B}} - 2\left(1-B^2\right)^{1/2}. \qquad (43)$$

The alternative signs in (42) correspond to the cases $B > 1$ or $B < -1$. Next, the trailing shelf is found from (37, 38) where

$$B^2 > 1: \quad M_0 = \pm|\frac{6\lambda}{\beta}|^{1/2} 4\text{arctan}\sqrt{\frac{B-1}{B+1}}, \qquad (44)$$

$$0 < B < 1: \quad M_0 = \pm|\frac{6\lambda}{\beta}|^{1/2} 4\text{arctanh}\sqrt{\frac{1-B}{1+B}}. \qquad (45)$$

Here the alternative signs in (44) and (45) correspond to the cases $\alpha B > 0$ or $\alpha B < 0$.

The expression (40) provides an explicit formula for the dependence of B on the basic state parameters α, β, λ, ν. It is readily shown that $G(B)$ (42) is a monotonically increasing function of $|B|$ for $1 < |B| < \infty$, and is a monotonically decreasing function of B for $0 < B < 1$ (43). Thus as $|\beta^3/\lambda\alpha^2| \to \infty$, then so does $G(B)$. If $\beta < 0$ so that $0 < B < 1$, $B \to 0$ and the wave approaches the limiting "table-top" shape. On the other hand if $\beta > 0$ and $1 < |B| < \infty$ then $|B| \to \infty$ and the wave shape approaches the "sech"-profile, The behaviour of the wave amplitude in these limits depends on the behaviour of each of the parameters α, β, λ. But since we can usually expect β to be finite and $\lambda(>0)$ to be non-zero, we see that these limiting shapes are usually achieved at the critical point where $\alpha \to 0$. This case is discussed below in Sect. 3.2. On the other hand, if $|\beta^3/\lambda\alpha^2| \to 0$, then so does $G(B)$. In this case $B \to 1$, $G(B) \sim |B-1|^{3/2}$ (see (42, 43)) and the wave profile reduces to the KdV "sech^2"-shape, provided that either $\beta < 0$ when $0 < B < 1$, or if $\beta > 0$, then the wave belongs to the branch defined by $1 < B < \infty$. These scenarios are usually achieved at the alternative critical point where $\beta = 0$, discussed below in Sect. 3.2.

3.2 Passage through a critical point

The adiabatic deformation of a solitary wave discussed above in Sect. 3.1 shows that the critical points where $\alpha = 0$, or where $\beta = 0$, are sites where we may anticipate a change in the wave structure. First we recall the vKdV model (3) where $\beta = 0$. In this case the adiabatic law (40) collapses to $a^3 \propto \alpha/\lambda$ where a is the solitary wave amplitude (19), and the expression (37) collapses to $D_1 = a_\sigma/2\lambda K^3$. Suppose that $\alpha = 0$ at $\sigma = 0$, where, without loss of generality, we can assume that α passes from a negative to a positive value as σ increases through zero. Initially the solitary wave is located in $\sigma < 0$ and has negative polarity, corresponding to the usual oceanic situation. Then, near the transition point, the amplitude of the wave decreases to zero as $a \sim -|\alpha|^{1/3}$, while $K \sim |\alpha|^{2/3}$; the momentum of the solitary wave is of course conserved (to leading order), but the mass of the solitary wave increases (in absolute value) as $1/|\alpha|^{1/3}$, its speed decreases as $|\alpha|^{4/3}$, and the amplitude $D_1 > 0$ of the trailing shelf just behind the solitary wave grows as $|\alpha|^{-8/3}$; the total mass of the trailing shelf is positive and grows as $1/|\alpha|^{1/3}$, in balance with the negative mass of the solitary wave, while the total mass remains a negative constant. Since the tail grows to be comparable with the wave itself, the adiabatic approximation breaks down as the critical point is approached. Nevertheless, we can infer that the the solitary wave itself is destroyed as the wave passes through the critical point $\alpha = 0$. The structure of the solution beyond this critical point has been examined numerically by Knickerbocker and Newell (1980) and revisited by Grimshaw et al. (1998a), who showed that the shelf passes through the critical point as a positive disturbance, which then being in an environment with $\alpha > 0$, can generate a train of solitary waves of positive polarity, riding on a negative pedestal, see Fig. 3.

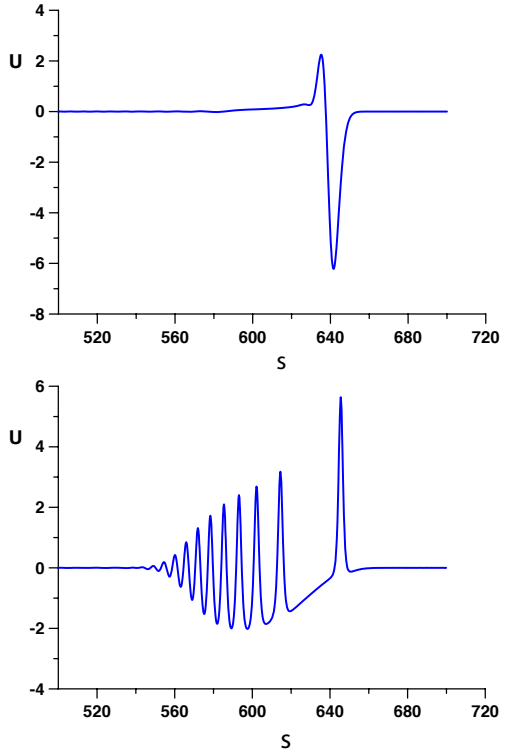

Fig. 3. Numerical simulation of the vKdV equation (3) with $\delta = 1$ and as α varies from -1 to +1. The upper panel is when $\alpha = 0$ and the lower panel is when $\alpha = 1$. The simulation shows a strong deformation of the initial solitary wave of depression at $\alpha = 0$, followed at $\alpha = 1$ by the emergence of a number of solitary waves of elevation riding on a negative pedestal.

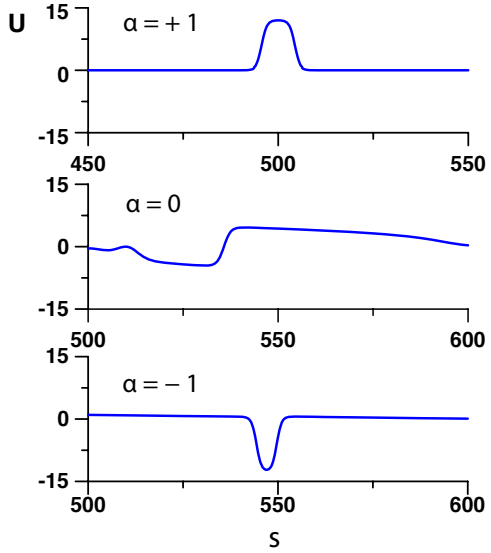

Fig. 4. Numerical simulation of the evKdV equation (6) with $\delta = 1$, $\beta = -0.083$ and as α varies from 1 to -1. The upper panel shows the initial condition of a "table-top" solitary wave of elevation at $\alpha = -1$, the middle panel shows a strong deformation at $\alpha = 0$, and the lower panel shows the leading wave at $\alpha = -1$. This wave is a "table-top" wave of depression riding on a small positive pedestal.

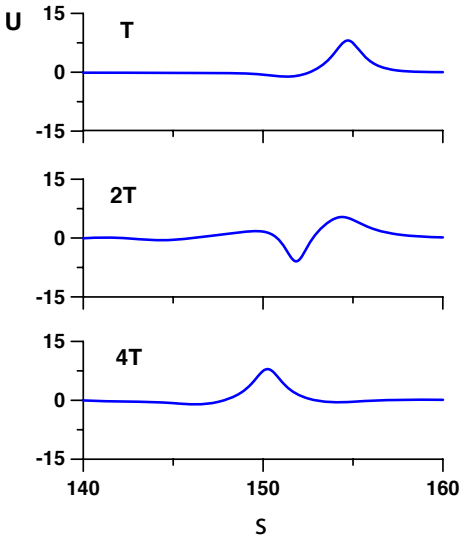

Fig. 5. Numerical simulation of the evKdV equation (6) for the case when $\delta = 1$, $\beta = 0.3$, $\nu = 0$ and α varies from 1 to -1. The initial wave (not shown) is a solitary wave of elevation belonging to the branch for which $B > 0$. It then passes adiabatically through the critical point, changing the sign of B to $B < 0$, and arrives at the location $\alpha = -1$ where $\xi = T$ with only a small deformation. However, at this stage its amplitude is below that allowed for a steady solitary wave, and so it deforms into a breather, shown in the middle panel for $\xi = 2T$ and the lower panel for $\xi = 4T$.

We next take account of the cubic nonlinear term in (6) and suppose again that α passes through zero at $\sigma = 0$ but that $\beta \neq 0$ at the critical point. First, let us suppose that $\beta < 0$, $0 < B < 1$. Then as $\alpha \to 0$, we see from (40) and (43) that $G(B) \sim 1/|\alpha|$, and $B \to 0$ with $B \sim 2\exp(-G/2)$. Thus the approach to the limiting "table-top" wave is quite rapid. From (31) $K \sim |\alpha|$ in this limit, and the amplitude approaches the limiting value $a \sim -\alpha/\beta$. Thus the wave amplitude decreases to zero, and, interestingly, this is a more rapid destruction of the solitary wave than for the case when $\beta = 0$. The mass M_0 (45) of the solitary wave grows as $|\alpha|^{-1}$ and so the amplitude D_1 of the trailing shelf (37) grows as $1/|\alpha|^4$. The overall scenario after α has passed through zero is similar to that described above for the vKdV equation (3) and has been discussed in detail by Grimshaw et al. (1999); see Fig. 4 for a case when a "table-top" solitary wave is converted to another such wave of opposite polarity, riding on a pedestal.

Next, let us suppose that $\beta > 0$ so that $1 < |B| < \infty$ There are two sub-cases to consider, $B > 0$ or $B < 0$, when the the solitary wave has the same or opposite polarity to α. Then as $\alpha \to 0, |B| \to \infty$ as $|B| \sim 1/|\alpha|$. It follows from (31) that then $K \sim 1$, $D \sim 1/|\alpha|, a \sim 1$, $M_0 \sim 1$. It follows that the wave adopts the "sech"-profile, but has *finite* amplitude, and so can pass through the critical point $\alpha = 0$ without destruction. But the wave changes branches from $B > 0$ to $B < 0$ as $|B| \to \infty$, or vice versa. An interesting situation then arises when the wave belongs to the branch with $-\infty < B < -1$ and the amplitude is reducing. If the limiting amplitude of $-2\alpha/\beta$ is reached, then there can be no further reduction in amplitude for a solitary wave, and instead a breather will form. An example of this outcome is shown in Fig. 5, where the wave has entered this regime after passing through the critical point.

Finally, consider the case when $\beta \to 0$, $\alpha \neq 0$. This case has been studied by Nakoulima et al. (2004) using both an asymptotic analysis similar to that used here, and numerical simulations. As already noted above, in this case $B \to 1$, $G(B) \sim |B-1|^{3/2}$ (42, 43), and it then follows from (40) that $G \sim |\beta|^{3/2}$ and so $|B-1| \sim |\beta|$. There are three sub-cases to consider. First, suppose that initially $\beta < 0$ and so $0 < B < 1$. As $|\beta| \to 0$, $1 - B \sim |\beta|$ and the wave profile becomes the familiar KdV "sech^2"-shape. It is readily shown from (31) that then K, a, M_0, $D_1 \sim 1$ and so the wave can pass through the critical point $\beta = 0$ without destruction. However, after passage through the critical point, the wave has moved to a different solitary branch (see Fig. 2), and this may change its ultimate fate. A typical scenario is shown in Fig. 6, which shows the transformation of a "table-top" solitary wave (upper panel in Fig. 2) to a KdV "sech^2"-KdV solitary wave at the critical point, and further evolution as a solitary wave of the upper branch in the lower panel of Fig. 2. Second, suppose that initially $\beta > 0$ and $1 < B < \infty$. Now $B - 1 \sim \beta$ and again the wave profile becomes the familiar KdV "sech^2"-shape, while K, a, M_0, $D_1 \sim 1$,

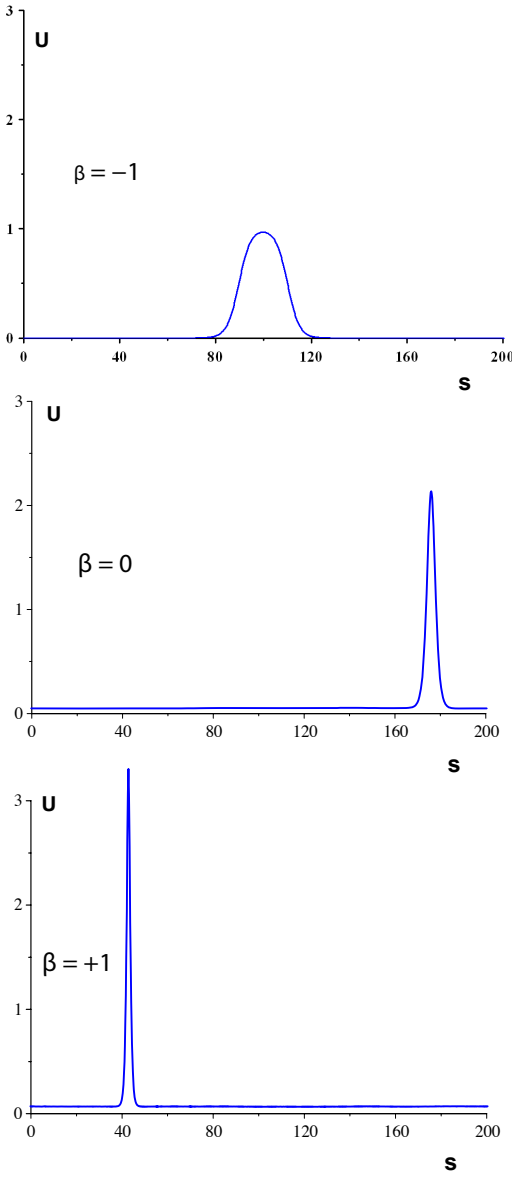

Fig. 6. Numerical simulation of the evKdV equation (6) with $\alpha = 1$, $\lambda = 1$ and β varies from -1 to 1, showing the transformation of a "table-top" solitary wave to a KdV "sech^2"-KdV solitary wave at the critical point, and further evolution as a solitary wave tending to a "sech"-profile.

allowing the wave to pass through the critical point $\beta = 0$ without destruction, but moving now from the upper branch in the lower panel of Fig. 2 to the "table-top" branch in the upper panel of Fig. 2. Third, suppose that initially $\beta > 0$ and $-1 > B > -\infty$. In this case it an be shown from (42) that $G(B)$ decreases from ∞ to a finite value of 2π as B increases from $-\infty$ to -1. Consequently the limit $\beta \to 0$ in (40) cannot be achieved. Instead as β decreases the limit $B = -1$ is reached, when the wave becomes an algebraic solitary wave, and a further decrease in β generates a breather.

4 Application to internal solitary waves in the South China Sea

In a typical oceanic situation, where there is a relatively sharp near-surface pycnocline, an internal solitary wave of depression is generated in the deep water and propagates shorewards until it reaches a critical point. For a simple two-layer model, this is where the pycnocline is close to the mid-depth, see (24). The theory described above then predicts that this wave will be destroyed in the vicinity of this critical point and replaced in the shallow water shorewards of the critical point by one or more internal solitary waves of elevation riding on a negative pedestal. This basic scenario has been observed in several places in the ocean, For instance, this phenomena has been reported by Salusti et al. (1989) in the Eastern Mediterranean, by Holloway et al. (1997, 1999) and Grimshaw et al. (2004) in the North West Shelf of Australia, by Hsu et al. (2000) in the East China Sea, during the ASIAEX experiment in the South China Sea by Duda et al. (2004), Liu et al. (1998, 2004), Orr and Mignerey (2003), Ramp et al. (2004), Yang et al. (2004), Zhao et al. (2003, 2004) and Zheng et al. (2003), and on the New Jersey shelf by Shroyer et al. (2009). Further, numerical simulations of the full Euler equations predict polarity reversal in Lake Constance (Vlasenko and Hutter, 2002), in the Andaman Sea (Vlasenko and Staschuk, 2007) and in the Saint Lawrence estuary (Bourgault et al., 2007). But elsewhere in the ocean, where there are no such critical points, the shoreward propagating small-amplitude internal solitary waves are expected to deform adiabatically (at least within the framework of the vKdV equation). Examples of this behaviour occur on the Malin Shelf off the North West coast of Scotland (Small, 2003; Grimshaw et al., 2004; Small and Hornby, 2005), in the Laptev Sea in the Arctic (Grimshaw et al., 2004) and in the COPE experiment on the Oregon shelf (Vlasenko et al., 2005).

The South China Sea (SCS) is well known as a location where internal solitary waves have been commonly observed, and has been intensively studied both experimentally and through numerical simulations, see for instance the reports based on the 2001 ASIAEX experiments by Duda et al. (2004), Ramp et al. (2004) and Liu et al. (2004). Typically, large amplitude internal waves are generated by the barotropic tidal currents, possibly combined with the Kuroshio current extension, interacting with the topography in Luzon Strait, see Liu et al. (1998), Cai et al. (2002), Ramp et al. (2004, 2006). Solitary-like waves with amplitudes up to 80 m (in a depth of 300 m) have been observed at the two underwater mountain ridges in Luzon Strait, see the bathymetry in Fig. 7 and the wave field in Fig. 8, taken from Liu et al. (2006). These waves cross the deep basin and then shoal on the continental shelf in water of depth 400–200 m, see for example the reports of the ASIAEX experiment by Duda et al. (2004), Ramp et al. (2004) and Liu et al. (2004). Wave amplitudes can reach to 100 m

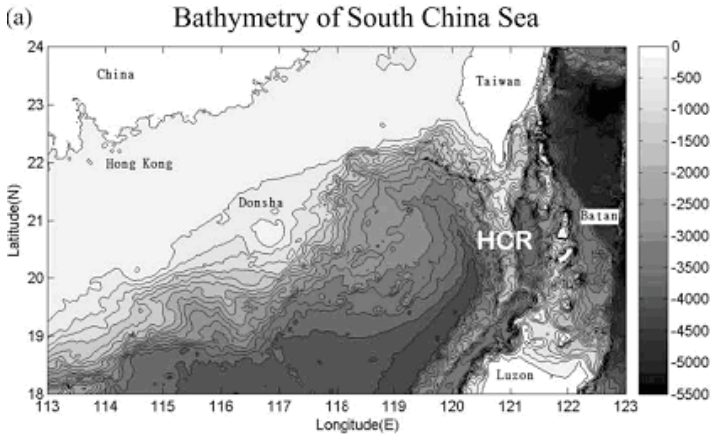

Fig. 7. Bathymetry of the northern part of the South China Sea, from Liu et al. (2006).

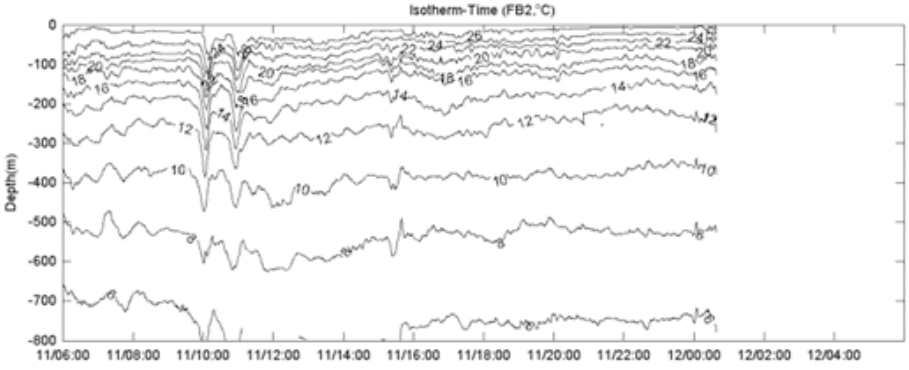

Fig. 8. Displacement of the isotherms as measured in the South China Sea, from Liu et al. (2006).

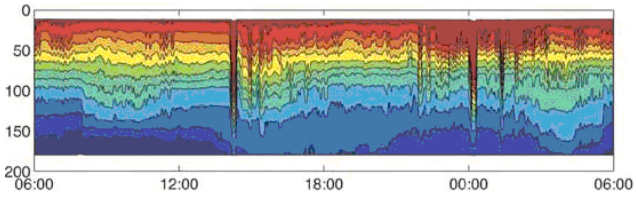

Fig. 9. Time series of internal waves in the South China Sea, from Duda et al. (2004).

and their shapes compare well with theoretical solitary wave shapes, see Klymak et al. (2006) and Fig. 9 from Liu et al. (2006). Numerical modeling of internal solitary wave transformation on the continental slope and shelf of the SCS has often been based on the vKdV and evKdV models, using mainly two-layer representations of the density stratification, and the results have been used to interpret the observed solitary wave evolution and especially the observed polarity changes, see Orr and Mingerey (2003), Zhao et al. (2003, 2004), Liu et al. (1998, 2004). There are also a few numerical simulations using the full Euler equations for stratified flow, see Buijsman et al. (2008), Du et al. (2008), Scotti et al. (2008), Warn-Varnas et al. (2010) and Vlasenko et al. (2010) for instance.

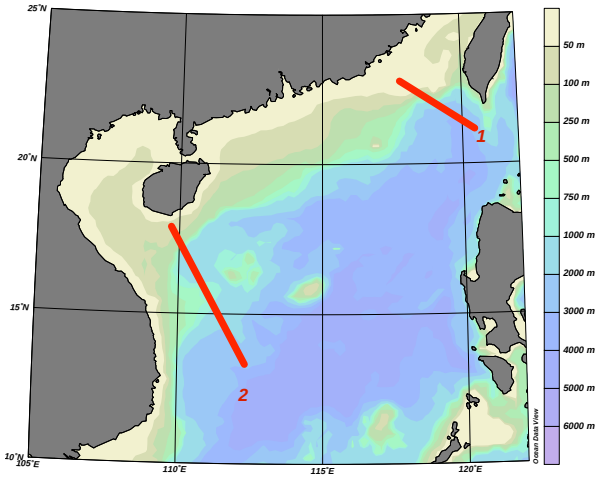

Fig. 10. Bathymetry of the South China Sea, with the chosen cross-sections.

We shall supplement these studies by a set of numerical simulations of the evKdV equation (6) for two typical cross-sections of the SCS, shown in Fig. 10. The first cross-section is close to the conditions for ASIAEX 2001, where the internal solitary waves are generated by westward tidal

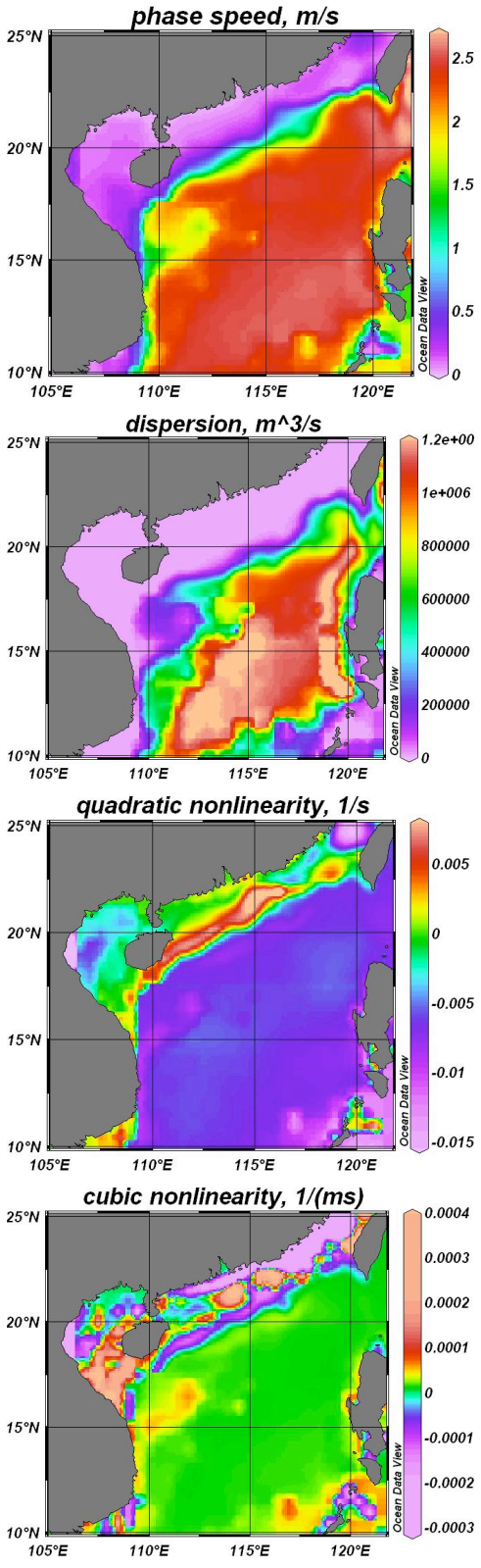

Fig. 11. Contour maps of the coefficients of the evKdV equation for the South China Sea. The plots are those for the phase speed c, the dispersion coefficient δ, the quadratic coefficient μ, and the cubic coefficient μ_1.

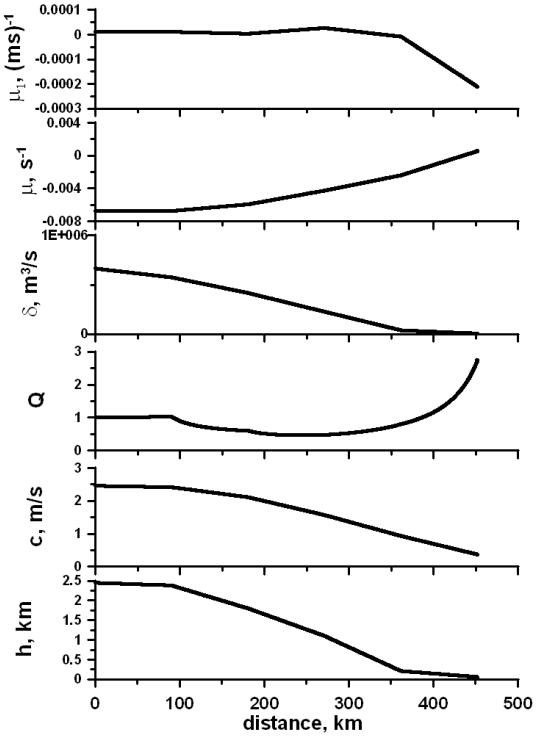

Fig. 12. Coefficients of the evKdV equation (5) along cross-section 1.

currents in Luzon Strait, see Liu et al. (2006) and Zhao and Alford (2006) for instance. The second cross-section is chosen to have a positive cubic nonlinear coefficient along the whole wave path. Contour maps of the linear long wave speed, the coefficients of the quadratic and cubic nonlinear terms and the coefficient of the linear dispersive term in the evKdV equation (5) are shown on Fig. 11. They are based on the vertical density profiles from the database GDEM for January (GDEM), while the bathymetry is taken from GEBCO. The speed c and the dispersion coefficient δ correlate well with the depth h as expected, see Talipova and Polukhin (2001) and Polukhin et al. (2003). The quadratic nonlinear coefficient μ is negative in the deep part of the SCS, and changes its sign to positive everywhere on the continental slope, as expected in the SCS, see Orr and Mignerey (2003) and Zhao et al. (2003, 2004) for instance. The cubic nonlinear coefficient, μ_1 is very small and positive in the deep part of the sea, but its sign changes in some parts of the continental slope to negative, while in other places it stays positive and grows in absolute value. To understand the role of quadratic and cubic nonlinearity in internal wave dynamics three values should be compared, c, μA, $\mu_1 A^2$. In the deep part of the SCS $c = 2.5\,\mathrm{m\,s^{-1}}$ and even if the internal wave amplitude is taken as 80 m (usually much less in deep water) $\mu A = 0.48\,\mathrm{m\,s^{-1}}$ and $\mu_1 A^2 = 0.13\,\mathrm{m\,s^{-1}}$; hence nonlinear effects are small in the deep part of the SCS. But on the continental slope c is less than $0.5\,\mathrm{m\,s^{-1}}$ and for the same

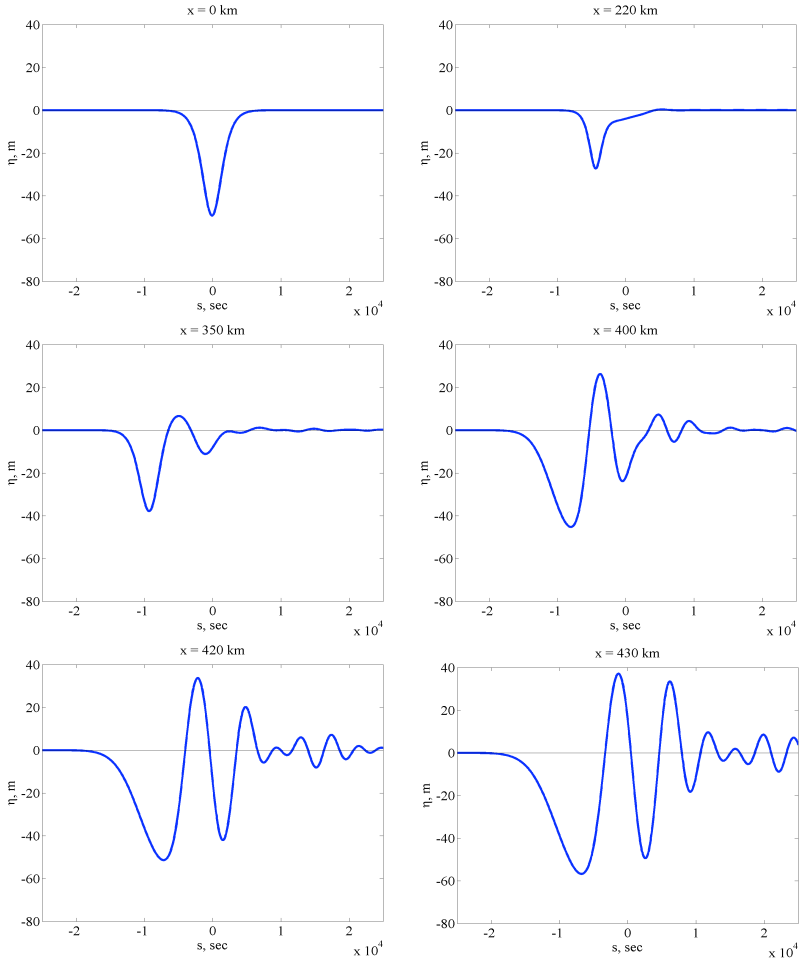

Fig. 13. Transformation of an internal solitary wave along cross-section 1.

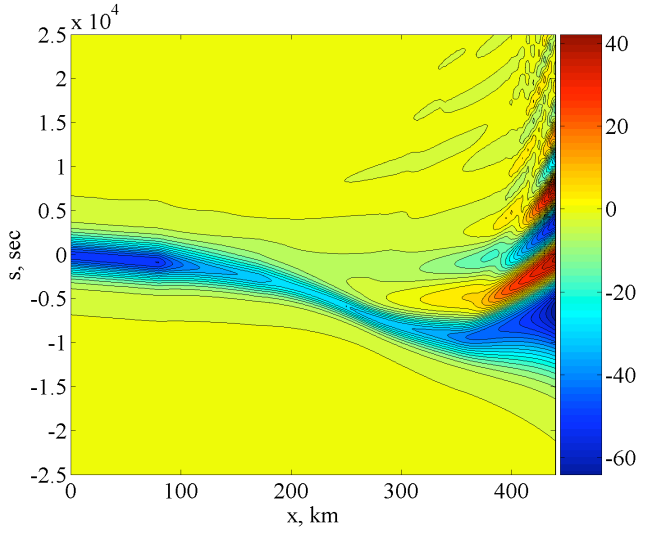

Fig. 14. Contour plot in the space-time domain of an internal solitary wave transformation along cross-section 1.

internal wave amplitude of about 80 m, $\mu A = 0.48\,\mathrm{m\,s^{-1}}$, comparable with c, and $\mu_1 A^2 = 1.28\,\mathrm{m\,s^{-1}}$, much large than the quadratic nonlinear term. Thus in the the shelf zones the waves are strongly nonlinear. Indeed the ratio of the nonlinear terms to the speed of propagation is about 3.5. Nevertheless, the eKdV (Gardner) model may be used as demonstrated by Maderich et al. (2009, 2010). However, it is pertinent to note that several other higher-order KdV-type models have been proposed, see the recent review by Apel et al. (2007) for instance.

4.1 Numerical results for cross-section 1

The wave path is close to the conditions of the ASIAEX 2001 experiment on the shelf (Ramp et al., 2004) and is here extended to the Luzon Strait to the site where the westward propagating solitary waves were observed see (Liu et al., 2006; Zhao and Alford, 2006 for instance). The model coefficients are shown on Fig. 12. The depth decreases from 2.5 km to 200 m, the linear long wave speed c varies from

$2.5\,\mathrm{m\,s^{-1}}$ to $0.2\,\mathrm{m\,s^{-1}}$, the linear modification factor Q is equal to 1 initially, then decreases to 0.5 at the location $x = 250$ km, before increasing to 2.5 on the shelf. Corresponding to the change of depth, the dispersion coefficient δ decreases along the cross-section. The nonlinear quadratic coefficient μ is negative for most of the wave path, but changes sign once only at a depth about 100 m. The cubic nonlinear coefficient μ_1 is positive in the deep water and becomes negative at a depth of about 400 m. Hence here there are two critical points, both on the shelf. The amplitude of the initial solitary wave (17) is chosen as 49 m at $x = 0$ in Fig. 14. This is less than that mentioned by Liu et al. (2006) where the amplitude of an observed solitary wave was estimated as 140 m, but it is large enough for our purposes.

The solitary wave evolution is shown in Fig. 13. The leading wave amplitude has decreased by a factor of two at $x = 220$ km from 49 m to 25 m. Over this same distance, the cubic nonlinear coefficient is almost constant, the quadratic nonlinear coefficient has decreased, the dispersive coefficient has decreased, while the linear modification factor has decreased by a factor of one-half; together these have the effect that the initial wave has started to deform with formation of a trailing tail. At the location $x = 350$ km the linear modification factor is decreasing, the cubic nonlinear coefficient changes sign and quadratic nonlinear coefficient tends to zero. The leading solitary wave now has an amplitude of about 35 m and is wider than at the location $x = 220$ km. At $x = 400$ km the quadratic nonlinear coefficient changes sign, and we see the typical destruction of the negative solitary wave, and the consequent generation of several positive solitary waves. The space-time contour plot of this internal wave transformation is shown in Fig. 14.

4.2 Numerical results for cross-section 2

On this cross-section, the initial point lies in deep water of depth $h = 3$ km, and the last point lies near Hainan Island. Here, the cubic nonlinear coefficient is positive everywhere, while the quadratic nonlinear coefficient changes sign on the shelf. The model coefficients are shown in Fig. 15. The depth decreases from 3 km to 200 m non-monotonically, producing the analogous tendencies for the dispersion coefficient δ, and the linear long wave speed c. The linear modification factor Q is initially close to one, and then decreases before increasing after the location $x = 700$ km. The quadratic coefficient μ grows after $x = 400$ km in absolute value and after $x = 580$ km tends to zero, changing sign at the location $x = 700$ km. The cubic coefficient μ_1 is positive everywhere, but grows by an order of magnitude.

This is a scenario when we might expect the formation of a breather from a solitary wave at the location of where the quadratic coefficient changes sign, provided the leading wave amplitude is large enough. Here we did two runs with initial solitary wave amplitudes of 23 m and 41 m. The solitary wave transformation for the first run is shown in Fig. 16. Due to the increase of the cubic nonlinear coefficient the initial solitary wave becomes narrower and a trailing tail emerges, developing oscillations after $x = 600$ km. This process occurs without a significant change in the leading wave amplitude because the modification factor increases slowly. At the location $x = 700$ km a "sech"-like solitary wave has appeared. Then, at the location $x = 730$ km the quadratic nonlinear coefficient changes sign, but the leading wave amplitude is then not large enough for transformation into a "sech"-like solitary wave of negative polarity, but with a positive quadratic coefficient. Instead, the wave disintegrates and at the location $x = 760$ km, we see the formation of secondary solitary waves of opposite polarity. The space-time contour plot of this run is shown in Fig. 17.

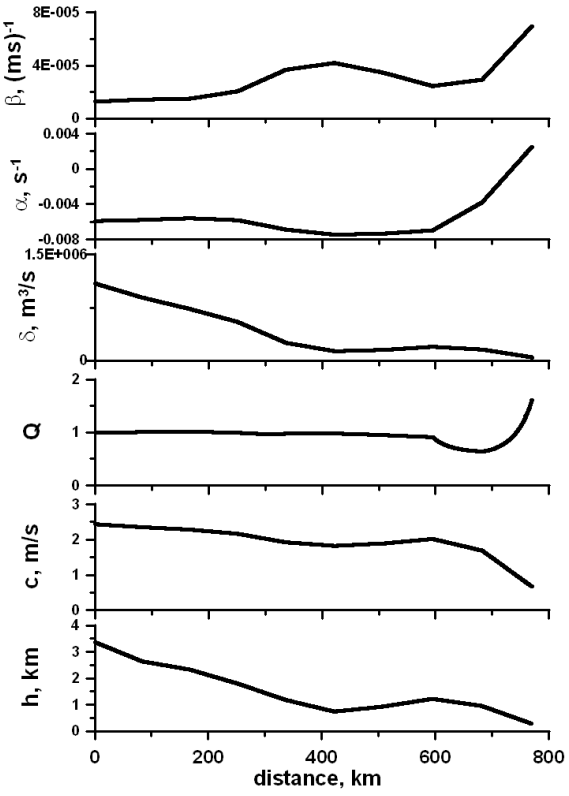

Fig. 15. Coefficients of the evKdV equation (5) along cross-section 2.

The second run has an initial amplitude of 41 m. The solitary wave transformation is shown in Fig. 18. Again a "sech"-like solitary wave forms by the location $x = 500$ km, and its amplitude grows to 60 m. At the location $x = 600$ m a second solitary waves begins to form, and due to the increase of the linear modification factor Q, the amplitude of leading wave decreases to about 45 m. Then as the quadratic nonlinear coefficient tends to zero, the cubic nonlinear coefficient grows rapidly, and the leading solitary wave begin to destruct around the location $x = 700$ km, until at the location $x = 720$ km there is a strong indication that an internal breather has formed in association with an

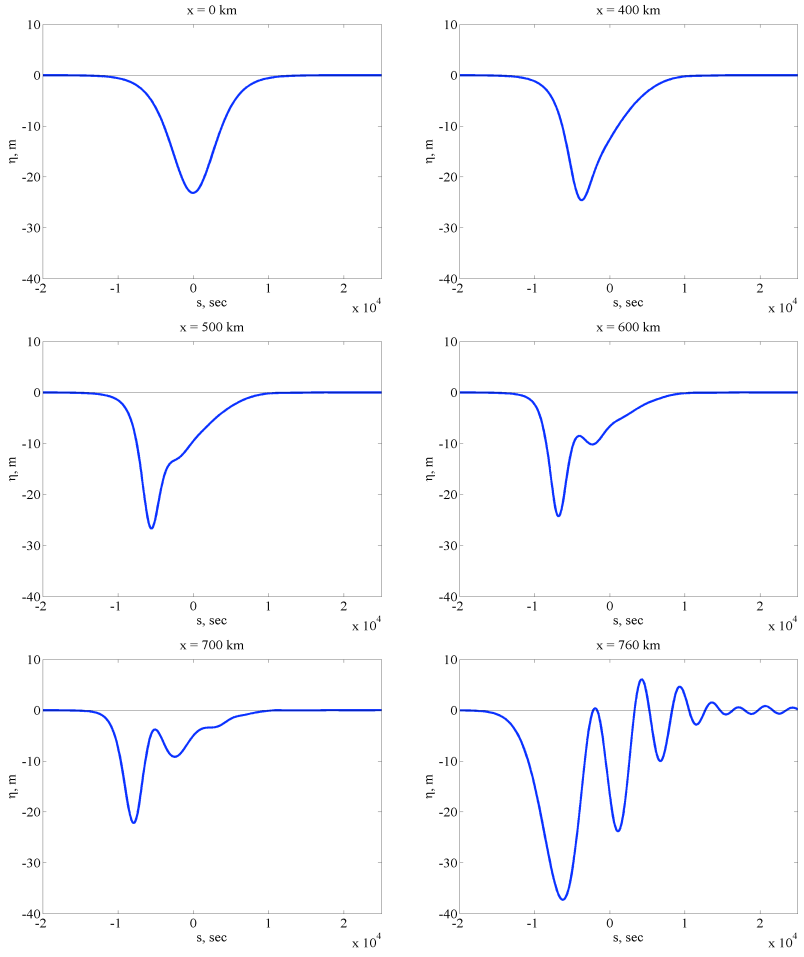

Fig. 16. Transformation of an internal solitary wave along cross-section 2, initial amplitude 23 m.

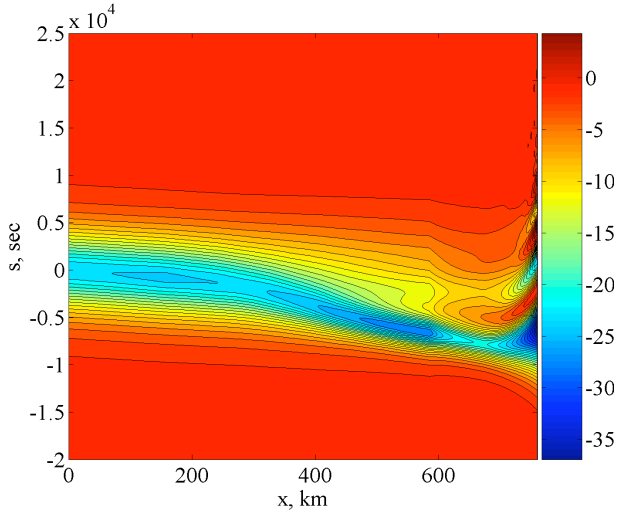

Fig. 17. Transformation of an internal solitary wave along cross-section 2, initial amplitude 23 m.

oscillatory trailing wave train. The division of the initial solitary wave into two is clearly shown in the space-time contour plots in Fig. 19, from the location $x = 400$ km to the location $x = 650$ km, with breather formation after $x = 700$ km.

5 Discussion

As we have mentioned in the Introduction, the vKdV equation (3) and its extension to allow for cubic nonlinearity, the evKdV equation (6) have been widely used to model the propagation of large amplitude internal solitary waves in coastal seas. In this review article we have presented a brief outline of the derivation of these models by an asymptotic expansion from the full Euler equations. Then we have described how an examination of the slowly-varying solitary wave solutions lead to the concept that the critical point where the coefficient of the quadratic, or of he cubic, nonlinear term is zero defines a location of special interest where a solitary wave may undergo a dramatic transformation, often involving a polarity change

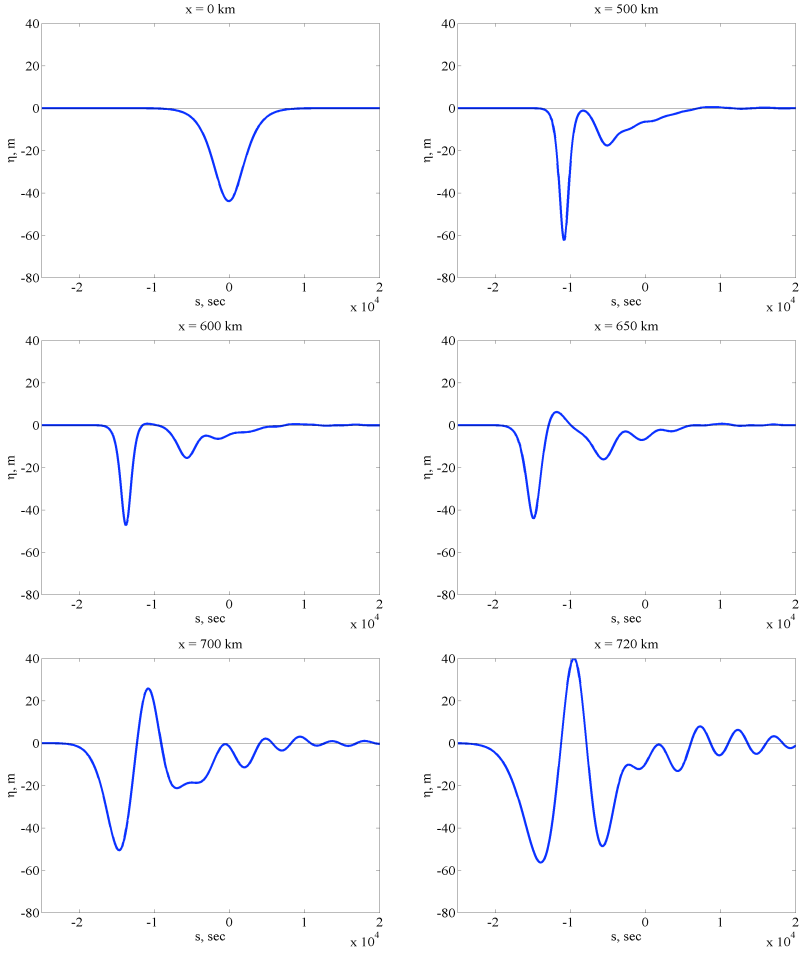

Fig. 18. Transformation of an internal solitary wave along cross-section 2, initial amplitude 41 m.

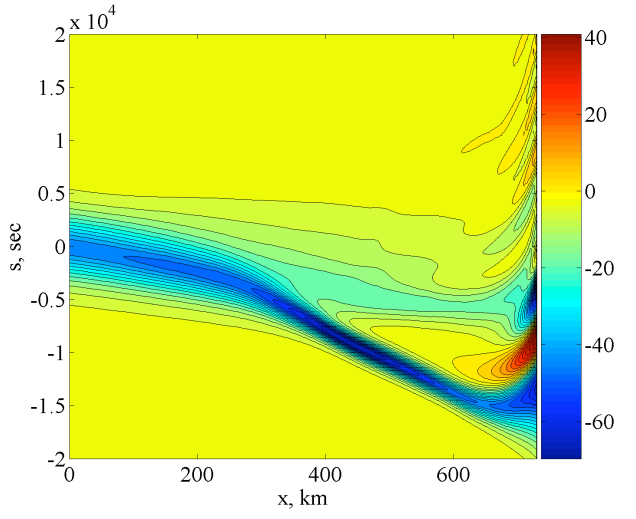

Fig. 19. Contour plot in the space-time domain of an internal solitary wave transformation along cross-section 2, initial amplitude 41 m.

and a disintegration into a wave train. We have illustrated this in detail for two contrasting cross-sections of the coastal shelf of the South China Sea. Each cross-section is based on the GDEM database of sea stratification, and the bathymetry database GEBCO. The first cross-section is taken across the shelf where the ASIAEX 2001 experiment took place, and we have simulated the transformation of an internal solitary wave generated in the Luzon Strait, propagating across the cross deep part of the sea to the opposite shelf, where a change in its polarity takes place, The second cross-section is taken across a region where the cubic nonlinear coefficient is positive everywhere. In this case an initial solitary wave of moderate amplitude transforms into two solitary waves. Th first wave is a ”sech”-like solitary wave, and the two waves interact near the location where the quadratic nonlinear coefficient changes sign, with transformation into a breather This demonstrates the possibility of internal breather generation from an initial solitary wave in a realistic ocean situation. It is the the second example of such a transformation, the first being a simulation for the North West Australian Shelf, see Grimshaw et al. (2007).

There are several important issues relating to internal solitary waves, which we have not considered here, notably stability, transverse structure, the effect of the background earth rotation and the effect of friction. An extension of the evKdV model (6) which takes into account of the last three factors could be

$$\left\{A_t + cA_x - \frac{cQ_x}{Q}A + \mu A\,A_x + \mu_1 A^2 A_x + \delta A_{xxx} + \nu|A|A\right\}_x + \frac{c}{2}\left(A_{yy} - \frac{f^2}{c^2}A\right) = 0. \quad (46)$$

The transverse term A_{yy} is just that which converts the KdV equation into its well-known two-dimensional extension, the KP equation, while the rotation term contains the Coriolis parameter f and was originally introduced by Ostrovsky (1978) and later by Grimshaw (1985) with the transverse term added as well. It is known that the effect of background rotation is to cause a solitary wave to decay through the radiation of inertia-gravity waves, see the review by Helfrich and Melville (2006) and the recent studies by Grimshaw and Helfrich (2008) and Sánchez-Garrido and Vlasenko (2009). In practice, the time-scale for this decay is one or two inertial periods. In (46) we have chosen Chezy friction, as this is the one most commonly used, although other forms of friction such as boundary-layer friction or Burgers-type friction have been proposed. The friction coefficient is given by

$$I\nu = \rho_0 C_D (c-u_0)^2 |\phi_z|^3, \text{ at } z=-h, \quad (47)$$

where C_D is the usual drag coefficient, while the modal functions and the integral I are defined by (10, 11, 15). Clearly friction will cause the solitary wave to decay, but as oceanic internal solitary waves are observed to be long-lived, this decay is evidently quite slow. There have been several recent observational studies of the decay of shoaling internal solitary waves from which we infer that the time scale is around an inertial period, and the decay process itself is complicated by the generation of localized shear instability, see for instance Moum et al. (2007) and Shroyer et al. (2010). We also note the interesting theoretical prediction by Grimshaw et al. (2003) that a decaying solitary wave with the parameter $B < -1$ (which requires that $\delta\mu_1 > 0$) may transform into a breather. Finally, we comment that although solitary waves are stable in the framework of the KdV or eKdV equations, in practice they can be unstable due to localized shear instability. This is a high-wavenumber phenomenon, which is not captured in the present long-wave asymptotic models. There have been several laboratory studies of shear instabiity of internal solitary waves, see Fructus et al. (2009) for a recent study, and several analogous ocean observations, see Moum et al. (2003, 2007).

Acknowledgements. This work was partially supported by grants RFBR 09-05-90408, 09-05-20024 (TT), and by RFBR 10-05-00199, Russian Grant for young scientists MK-846.2009.1 (O.K).

Edited by: V. I. Vlasenko
Reviewed by: Y. A. Stepanyants and two other anonymous referees

References

Apel, J., Ostrovsky, L. A., Stepanyants, Y. A., and Lynch, J. F.: Internal solitons in the ocean and their effect on underwater sound, J. Acoust. Soc. Am., 121, 695–722, 2007.

Benjamin, T. B.: Internal waves of finite amplitude and permanent form, J. Fluid Mech., 25, 241–270, 1966.

Benney, D. J.: Long non-linear waves in fluid flows, J. Math. Phys., 45, 52–63, 1966.

Bourgault, D., Blokhina, M. D., Mirchak, R., and Kelly, D. E.: Evolution of a shoaling internal solitary wave train, Geophys. Res. Lett., 34, L03601, doi:10.1029/2006GL028462, 2007.

Boussinesq, M. J.: Théorie de l'intumescence liquide appellée onde solitaire ou de translation, se propageant dans un canal rectangulaire, Comptes Rendus Acad. Sci., Paris, 72, 755–759, 1871 (in French).

Buijsman, M. C., Kanarska, Y., and McWilliams, J. C.: On the generation and evolution of nonlinear internal waves in the South China Sea, J. Geophys. Res., 115, C02012, doi:10.1029/2009JC005275, 2010.

Cai, S., Long, X., and Gan, Z.: A numerical study of the generation and propagation of internal solitary waves in the Luzon Strait, Oceanol. Acta, 25, 51–60, 2002.

Clarke, S., Grimshaw, R., Miller, P., Pelinovsky, E., and Talipova, T.: On the generation of solitons and breathers in the modified Korteweg-de Vries equation, Chaos, 10, 383–392, 2000.

Djordjevic, V. and Redekopp, L.: The fission and disintegration of internal solitary waves moving over two-dimensional topography, J. Phys. Oceanogr., 8, 1016–1024, 1978.

Du, T., Tseng, Y.-H., and Yan, X.-H.: Impacts of tidal currents and Kuroshio intrusion on the generation of nonlinear internal waves in Luzon Strait, J. Geophys. Res., 113, C08015, doi:10.1029/2007JC004294, 2008.

Duda, T. F., Lynch, J. F., Irish, J. D., Beardsley, R. C., Ramp, S. R., Chiu, C.-S., Tang, T. Y., and Yang, Y.-J.: Internal tide and nonlinear internal wave behavior at the continental slope in the northern south China Sea, IEEE J. Oceanic Eng., 29, 1105–1130, 2004.

El, G. A. and Grimshaw, R.: Generation of undular bores in the shelves of slowly-varying solitary waves, Chaos, 12, 1015–1026, 2002.

Fructus, D., Carr, M., Grue, J., Jensen, A., and Davies, P. A.: Shear induced breaking of large amplitude internal solitary waves, J. Fluid Mech., 620, 1–29, 2009.

Grimshaw, R.: Slowly varying solitary waves. I: Korteweg-de Vries equation, Proc. Roy. Soc. A, 368, 359–375, 1979.

Grimshaw, R.: Evolution equations for long nonlinear internal waves in stratified shear flows, Stud. Appl. Math., 65, 159–188, 1981.

Grimshaw, R.: Evolution equations for weakly nonlinear, long internal waves in a rotating fluid, Stud. Appl. Math., 73, 1–33, 1985.

Grimshaw, R.: Internal solitary waves. In: Environmental Stratified Flows, edited by: Grimshaw, R., Kluwer, Boston, Chapter 1, 1–28, 2001.

Grimshaw, R.: Internal solitary waves in a variable medium, Gesellschaft fur Angewandte Mathematik, 30, 96–109, 2007.

Grimshaw, R. and Mitsudera, H.: Slowly-varying solitary wave solutions of the perturbed Korteweg-de Vries equation revisited, Stud. Appl. Math., 90, 75–86, 1993.

Grimshaw, R., Pelinovsky, E., and Talipova, T.: Solitary wave transformation due to a change in polarity, Stud. Appl. Math., 101, 357–388, 1998a.

Grimshaw, R., Pelinovsky, E., and Talipova, T.: Solitary wave transformation in a medium with sign-variable quadratic nonlinearity and cubic nonlinearity, Physica D, 132, 40–62, 1999.

Grimshaw, R., Pelinovsky, E., and Poloukhina, O.: Higher-order Korteweg-de Vries models for internal solitary waves in a stratified shear flow with a free surface, Nonlin. Processes Geophys., 9, 221–235, doi:10.5194/npg-9-221-2002, 2002.

Grimshaw, R, Pelinovsky, E and Talipova, T.: Damping of large-amplitude solitary waves, Wave Motion, 37, 351–364, 2003.

Grimshaw, R. H. J. and Pudjaprasetya, S. R.: Generation of secondary solitary waves in the variable-coefficient Korteweg-de Vries equation, Stud. Appl. Math., 112, 271–279, 2004.

Grimshaw, R., Pelinovsky, E., Talipova, T., and Kurkin, A.: Simulation of the transformation of internal solitary waves on oceanic shelves J. Phys. Oceanogr., 34, 2774–2779, 2004.

Grimshaw, R., Pelinovsky, E., Stepanyants, Y., and Talipova, T.: Modelling internal solitary waves on the Australian North West Shelf, Mar. Freshwater Res., 57, 265–272, 2006.

Grimshaw, R., Pelinovsky, E., and Talipova, T.: Modeling internal solitary waves in the coastal ocean, Surv. Geophys., 28, 273–298, 2007.

Grimshaw, R. and Helfrich, K. R.: Long-time solutions of the Ostrovsky equation, Stud. Appl. Math., 121, 71–88, 2008.

Grimshaw, R., Slunyaev, A., and Pelinovsky, E.: Generation of solitons and breathers in the extended Korteweg-de Vries equation with positive cubic nonlinearity, Chaos, 20, 013102, doi:10.1063/1.3279480, 2010.

Helfrich, K. R. and Melville, W. K.: Long nonlinear internal waves, Annu. Rev. Fluid Mech., 38, 395–425, 2006.

Holloway, P., Pelinovsky, E., Talipova, T., and Barnes, B.: A nonlinear model of the internal tide transformation on the Australian North West Shelf, J. Phys. Oceanogr., 27, 871–896, 1997.

Holloway, P., Pelinovsky, E., and Talipova, T.: A generalised Korteweg-de Vries model of internal tide transformation in the coastal zone, J. Geophys. Res., 104, 18333–18350, 1999.

Holloway, P., Pelinovsky, E., and Talipova, T.: Internal tide transformation and oceanic internal solitary waves, in: Environmental Stratified Flows, edited by: Grimshaw, R., Kluwer, Boston, Chapter 2, 29–60, 2001.

Hsu, M.-K., Liu, A. K., and Liu, C.: A study of internal waves in the China Seas and Yellow Sea using SAR, Cont. Shelf Res., 20, 389–410, 2000.

Johnson, R. S.: On an asymptotic solution of the Korteweg-de Vries equation with slowly varying coefficients, J. Fluid Mech., 60, 813–824, 1973a.

Johnson, R. S.: On the development of a solitary wave moving over an uneven bottom, Proc. Camb. Philos. Soc., 73, 183–203, 1973b.

Klymak, J. M., Pinkel, R., Liu, Ch.-T., Liu, A. K., and David, L.: Prototypical solitons in the South China Sea, Geophys. Res. Lett., 33, L11607, doi:10.1029/2006GL025932, 2006.

Knickerbocker, C. J. and Newell, A. C.: Internal solitary waves near a turning point, Phys. Lett. A, 75, 326–330, 1978.

Knickerbocker, C. J. and Newell, A. C.: Shelves and the Korteweg-de Vries equation, J. Fluid Mech., 98, 803–818, 1980.

Korteweg, D. J. and de Vries, H.: On the change of form of long waves advancing in a rectangular canal, and on a new type of long stationary waves, Philos. Mag., 39, 422–443, 1895.

Lamb, K. G., Polukhina, O., Talipova, T., Pelinovsky, E., Xiao, W., and Kurkin, A.: Breather generation in fully nonlinear models of a stratified fluid, Phys. Rev. E, 75, 046306, doi:10.1103/PhysRevE.75.046306, 2007.

Liu, A. K., Chang, Y. S., Hsu, M.-K., and Liang, N. K.: Evolution of nonlinear internal waves in the East and South China Seas, J. Geophys. Res., 103, 7995–8008, 1998.

Liu, A. K., Ramp, S. R., Zhao, Y., and Tswen Yung Tang, T. Y.: A case study of internal solitary wave propagation during ASIAEX 2001, IEEE J. Oceanic Eng., 29, 1144–1156, 2004.

Liu, Ch.-T., Pinkel, R., Klymak, J., Hsu, M.-K., Chen, H.-W., and Villanoy, C.: Nonlinear internal waves from the Luzon Strait, EOS T. Am. Geophys. Un., 87, 449–451, 2006.

Maderich, V., Talipova, T., Grimshaw, R., Pelinovsky, E., Choi, B. H., Brovchenko, I., Terletska, K., and Kim, D. C.: The transformation of an interfacial solitary wave of elevation at a bottom step, Nonlin. Processes Geophys., 16, 33–42, doi:10.5194/npg-16-33-2009, 2009.

Maderich, V., Talipova, T., Grimshaw, R., Terletska, E., Brovchenko, I., Pelinovsky, E., and Choi, B. H.: Interaction of a large amplitude interfacial solitary wave of depression with a bottom step, Phys. Fluids, 22, 076602, doi:10.1063/1.3455984, 2010.

Moum, J. N., Farmer, D. M., Smyth, W. D., Armi, L., and Vagle, S.: Structure and generation of turbulence at interfaces strained by internal solitary waves propagating shoreward over the continental shelf, J. Phys. Oceanogr., 33, 2093–2112, 2003.

Moum, J. N., Farmer, D. M., Shroyer, E. L., Smyth, W. D., and Armi, L.: Dissipative losses in nonlinear internal waves propagating across the continental shelf, J. Phys. Oceanpgr., 37, 1989–1995, 2007.

Nakoulima, O., Zahibo, N., Pelinovsky, E., Talipova, T., Slunyaev, A., and Kurkin, A.: Analytical and numerical studies of the variable-coefficient Gardner equation, Appl. Math. Comput., 152, 449–471, 2004.

Orr, M. H. and Mignerey, P. C.: Nonlinear internal waves in the South China Sea: Observation of the conversion of depression internal waves to elevation internal waves, J. Geophys. Res., 108(C3), 3064, doi:10.1029/2001JC001163, 2003.

Ostrovsky, L.: Nonlinear internal waves in a rotating ocean, Oceanogology, 18, 119–125, 1978.

Ostrovsky, L. A. and Pelinovsky, E. N.: Wave transformation on the surface of a fluid of variable depth, Akad. Nauk SSSR, Izv. Atmos. Ocean Phys., 6, 552–555, 1970.

Ostrovsky, L. A. and Stepanyants, Y. A.: Internal solitons in laboratory experiments: Comparison with theoretical models, Chaos, 15, 037111, doi:10.1063/1.2107087, 28 pp., 2005.

Pelinovsky, D. and Grimshaw, R. H. J.: Structural transformation of eigenvalues for a perturbed algebraic soliton potential, Phys. Lett. A, 229, 165–172, 1997.

Polukhin, N., Talipova, T., Pelinovsky, E., and Lavrenov, I.: Kinematic characteristics of the high-frequency internal wave field in the Arctic, Oceanology, 43, 333–343, 2003.

Ramp, S. R., Tang, T. Y., Duda, T. F., Lynch, J. F., Liu, A. K., Chiu, C.-S., Bahr, F. L., Kim, H.-R., and Yang, Y.-J.: Internal solitons in the northeastern South China Sea, Part I: sources and deep water propagation, IEEE J. Oceanic Eng., 29, 1157–1181, 2004.

Rayleigh, J. W. S.: On waves, Philos. Mag., 1, 257–279, 1876.

Russell, J. S.: Report on Waves, 14th meeting of the British Association for the Advancement of Science, 311–390, 1844.

Salusti, F., Lascaratos, A., and Nittis, K.: Changes of polarity in marine internal waves: Field evidence in eastern Mediterranean Sea, Ocean Model., 82, 10–11, 1989.

Sánchez-Garrido, J. C. and Vlasenko, V.: Long-term evolution of strongly nonlinear internal solitary waves in a rotating channel, Nonlin. Processes Geophys., 16, 587–598, doi:10.5194/npg-16-587-2009, 2009.

Scotti, A., Beardsley, R. C., Butman, B., and Pineda, J.: Shoaling of nonlinear internal waves in Massachusetts Bay, J. Geophys. Res., 113, C08031, doi:10.1029/2008JC004726, 2008.

Shroyer, E. L., Moum, J. N., and Nash, J. D.: Observations of polarity reversal in shoaling nonlinear internal waves, J. Phys. Oceanogr., 39, 691–701, 2009.

Shroyer, E. L., Moum, J. N., and Nash, J. D.: Energy transformations and dissipation of nonlinear internal waves over New Jersey's continental shelf, Nonlin. Processes Geophys., 17, 345–360, doi:10.5194/npg-17-345-2010, 2010.

Small, J.: A nonlinear model of the shoaling and refraction of interfacial solitary waves in the ocean. Part I: Development of the model and investigations of the shoaling effect, J. Phys. Oceanogr., 31, 3163–3183, 2001a.

Small, J.: A nonlinear model of the shoaling and refraction of interfacial solitary waves in the ocean. Part II: Oblique refraction across a continental slope and propagation over a seamount, J. Phys. Oceanogr., 31, 3184–3199, 2001b.

Small, J. Refraction and shoaling of nonlinear internal waves at the Malin Shelf Break, J. Phys. Oceanogr., 33, 2657–2674, 2003.

Small, R. J. and Hornby, R. P.: A comparison of weakly and fully non-linear models of the shoaling of a solitary internal wave, Ocean Model, 8, 395–416, 2005.

Talipova, T. and Polukhin, N.: Averaged characteristics of the internal wave propagation parameters in the World Ocean, Izvestia of Russian Academy of Engineering Sciences, Series: Applied Mathematics and Informatics, 2, 139–155, 2001.

Vlasenko, V. I. and Hutter, K.: Transformation and disintegration of strongly nonlinear internal waves by topography in stratified lakes, Ann. Geophys., 20, 2087–2103, doi:10.5194/angeo-20-2087-2002, 2002.

Vlasenko, V. I., Stashchuk, N. M., and Hutter, K.: Baroclinic Tides: Theoretical Modelling and Observational Evidence, Cambridge University Press, Cambridge, 2005.

Vlasenko, V. I., Ostrovsky, L. A., and Hutter, K.: Adiabatic behaviour of strongly nonlinear internal solitary waves in slope-shelf areas, J. Geophys. Res., 110, C04006, doi:10.1029/2004JC002705, 2005.

Vlasenko, V. and Stashchuk, N.: Three-dimensional shoaling of large amplitude internal waves, J. Geophys. Res., 112, C11018, doi:10.1029/2007JC004107, 2007

Vlasenko, V., Stashchuk, N., Guo, C., and Chen, X.: Multimodal structure of baroclinic tides in the South China Sea, Nonlin. Processes Geophys., 17, 529–543, doi:10.5194/npg-17-529-2010, 2010.

Warn-Varnas, A., Hawkins, J., Lamb, K. G., Piacsek, S., Chin-Bing, S., King, D., and Burgos, G.: Solitary wave generation dynamics at Luzon Strait, Ocean Model., 31, 9–27, 2010.

Yang, Y.-J., Tang, T. Y., Chang, M. H., Liu, A. K., Hsu, M.-K., and Ramp, S. R.: Solitons northeast of Tung-Sha Island during the ASIAEX pilot studies, IEEE J. Oceanic Eng., 29, 1182–1199, 2004.

Zhao, Z., Klemas, V. V., Zheng, Q., Li, X., and Yan, X.-H.: Satellite observation of internal solitary waves converting polarity, Geophys. Res. Lett., 30(19), 1988, doi:10.1029/2003GL018286, 2003.

Zhao, Z., Klemas, V. V., Zheng, Q., Li, X., and Yan, X.-H.: Estimating parameters of a two-layer stratified ocean from polarity conversion of internal solitary waves observed in satellite SAR images, Remote Sens. Environ., 92, 276–287, 2004.

Zhao, Z. and Alford, M. H.: Source and propagation of internal solitary waves in the northeastern South China Sea, J. Geophys. Res., 111, C11012, doi:10.1029/2006JC003644, 2006.

Zheng, Q., Klemas, V., Yan, X.-H., and Pan, J.: Nonlinear evolution of ocean internal solitons propagating along an inhomogeneous thermocline, J. Geophys. Res., 106, 14083–14094, 2001.

Zheng, Q., Klemas, V., Zheng, Q., and Yan, X.-H.: Satellite observation of internal solitary waves converting polarity, Geophys. Res. Lett., 30(19), 4–1, 2003.

Zhou, X. and Grimshaw, R.: The effect of variable currents on internal solitary waves, Dynam. Atmos. Oceans., 14, 17–39, 1989.